Michael B. Sano[1]
Erin A. Henslee[1]
Eva Schmelz[2]
Rafael V. Davalos[1]*

[1]School of Biomedical Engineering and Sciences, Virginia Tech-Wake Forest University, Blacksburg, VA, USA
[2]College of Agriculture and Life Sciences, Virginia Tech, Blacksburg, VA, USA

Received June 30, 2011
Revised July 31, 2011
Accepted August 1, 2011

Research Article

Contactless dielectrophoretic spectroscopy: Examination of the dielectric properties of cells found in blood

The use of non-invasive methods to detect and enrich circulating tumor cells (CTCs) independent of their genotype is critical for early diagnostic and treatment purposes. The key to using CTCs as predictive clinical biomarkers is their separation and enrichment. This work presents the use of a contactless dielectrophoresis (cDEP) device to investigate the frequency response of cells and calculate their area-specific membrane capacitance. This is the first demonstration of a cDEP device which is capable of operating between 10 and 100 kHz. Positive and negative dielectrophoretic responses were observed in red blood cells, macrophages, breast cancer, and leukemia cells. The area-specific membrane capacitances of MDA-MB231, THP-1 and PC1 cells were determined to be 0.01518 $\pm$ 0.0013, 0.01719 $\pm$ 0.0020, 0.01275 $\pm$ 0.0018 (F/m^2), respectively. By first establishing the dielectrophoretic responses of cancerous cells within this cDEP device, conditions to detect and enrich tumor cells from mixtures with non-transformed cells can be determined providing further information to develop methods to isolate these rare cells.

Keywords:
Cancer detection / Clausius–Mossotti factor / Dielectrophoresis / Microfluidics / Sample isolation
DOI 10.1002/elps.201100351

1 Introduction

The use of non-invasive methods to detect and enrich cancer cells independent of their genotype is critical for early diagnostic and treatment purposes. In addition, isolation of these cells could provide a workbench for clinicians to screen drug therapies prior to patient treatment. This would enable oncologists to tailor treatment on a patient-specific level and to ensure that the most effective treatment is being utilized [1–5]. Since many symptoms associated with cancers can be attributed to multiple diseases, diagnosis must be accomplished via medical analysis. There are a number of molecular, cytogenic, immunological, cytochemical, and morphological assays capable of making this diagnosis; however, low proportions of cancerous cells make these processes challenging [6].

Correspondence: Associate Professor Michael B. Sano School of Biomedical Engineering and Sciences, Virginia Tech-Wake Forest University, 329 ICTAS Building, Stanger Street, MC 0298, Blacksburg, VA 24061 Office, USA
E-mail: sano@vt.edu
Fax: +1-540-231-9738

Abbreviations: AC, alternating current; **CTCs,** circulating tumor cells; **C-M,** Clausius–Mossotti; **cDEP,** contactless dielectrophoresis; **DEP,** dielectrophoresis

During progression, tumor cells acquire the capacity to disseminate into blood circulation until they are detected and eliminated by the immune system or until they attach to the endothelial cells, extravasate, and grow as secondary tumors (metastasis) at distant sites. These circulating tumor cells (CTCs) could serve as early indicators of cancer [7]. The most reliable method currently available for CTC detection is automated digital microscopy (ADM), which uses image analysis to recognize immunochemically or immunomagnetically labeled tumor cells. A study using the CellSearch System™ (Veridex LLC, Warren, NJ, USA), showed that the overall survival of patients with breast cancers harboring fewer than five CTCs in about 7 mL blood after 3–5 wk of starting their therapy was a relatively long 18.5 months. Women who had five CTCs or more had much shorter median survival times, ranging from 1.3 to 3.6 months [8, 9].

The majority of recent investigations have utilized qRT-PCR for the confirmation and genotyping of CTCs. This technique has been reported in the scientific literature as a valid method to confirm various CTCs derived from bladder [10], breast [11], lung [12], prostate [13, 14], and esophageal [15] cancers. Immunocytochemistry methods, using antibody–antigen identification are typically based on detection

*Additional corresponding author: Dr. Rafael V. Davalos
E-mail: davalos@vt.edu

Colour Online: See the article online to view Figs. 1 and 4 in colour.

of specific tumor or epithelial cell markers present in CTCs. While these are reliable methods, the specificity of CTC separation and their enrichment determines the quality of the results. The major drawback to this approach is that other cells, such as hematopoietic or fibroblasts cells, can express several epithelial markers such as keratins [16, 17], causing incomplete separation. Typically, more sensitive techniques may require prior knowledge of cell-specific markers and antibodies to prepare target cells for analysis. As result, there is a growing need for a marker-independent isolation and purification method to increase yield, sensitivity, precision, and reproducibility.

Dielectrophoresis (DEP), the motion of a particle in a non-uniform electric field, has become a robust method for analyzing nano-particles, cells, viruses, and DNA based on their physical and electrical properties [18]. Many devices exploit these DEP forces by placing metal electrodes in a microfluidic channel containing spatial non-uniformities (iDEP) [19–21] or via electrodes patterned on the channel floor (traditional DEP) [22]. Traditional DEP has been employed to separate breast cancer cells from blood [23]. Post-concentration analysis of cells enriched in these devices can be challenging, since cells must come in direct contact with the electrode and may be contaminated.

A new technique, contactless dielectrophoresis (cDEP) [24], utilizes fluid electrode channels which are isolated from a sample channel by a thin insulating membrane. When an alternating current (AC) voltage is applied, capacitive coupling between the sample and electrode channels produces the non-uniform electric field necessary for DEP. This technique has recently demonstrated the ability to isolate THP-1 human leukemia monocytes from a heterogeneous mixture of live and dead cells [25]. The absence of contact between electrodes and the sample prevents bubble formation and avoids any contaminating effects the electrodes may have on the sample.

The key to using CTCs as predictive clinical biomarkers is their separation and enrichment. By first establishing the DEP responses of normal and cancerous cells within this cDEP device, conditions to detect and enrich tumor cells from mixtures with non-transformed cells can be determined. This work is the first cDEP demonstration of both negative and positive DEP on mammalian cells. This is also the first demonstration of a cDEP device to investigate the electrical properties of cells. The frequency response of breast cancer, leukemia, macrophages, and red blood cells is investigated and their cell membrane capacitance is calculated. This method provides a simple way to interrogate the electrical properties of cells which will enable future cDEP designs to be specifically fabricated toward CTC detection within biological fluids.

2 Theory

Cells placed in an infinite ionic liquid under a non-uniform AC field become polarized and develop a charge distribution across the volume of the particle. Cells are then driven toward the regions of maximal field gradient by a translational DEP force ($\vec{F}_{\mathrm{DEP}}$) [26]

$$\vec{F}_{\mathrm{DEP}} = 2\pi\varepsilon_{\mathrm{m}} r^3 \mathrm{Re}[K(\omega)]\nabla(\vec{E}\cdot\vec{E})\cdot[\mathrm{N}] \quad (1)$$

where r is the radius of the cell, ε_{m} is the relative permittivity of the suspending medium, and Re[K(ω)] is the real part of the Clausius–Mossotti (C-M) factor. The C-M factor is a frequency-dependent ratio, with value between −0.5 and 1.0, dependent on the complex conductivity of the particle and the suspending medium. A particle-independent DEP vector can be defined as

$$\vec{\Gamma} = \frac{\vec{F}_{\mathrm{DEP}}}{2\pi\varepsilon_{\mathrm{m}} r^3 \mathrm{Re}[K(\omega)]} = \nabla(\vec{E}\cdot\vec{E})\cdot\left[\frac{\mathrm{V}^2}{\mathrm{m}^3}\right] \quad (2)$$

The single shell dielectric model introduced by Foster et al. [27] for the C-M factor can be used to describe a cell as a membrane-covered sphere with a membrane capacitance, C_{m}, suspended in a medium with conductivity, σ_{M}. The first frequency at which Re[K(ω)] = 0 is known as the first crossover frequency (f_{xo1}).

$$f_{\mathrm{xo1}} = \frac{\sqrt{2}\sigma_{\mathrm{M}}}{2\pi r C_{\mathrm{m}}}\cdot[\mathrm{Hz}] \quad (3)$$

At this frequency, the net DEP force acting on a cell will equal zero. Under the influence of an electric field at this frequency, the distribution of cells within the device will be identical to the case where no field is applied. Since this frequency can be determined experimentally and the cell radius and conductivity of the media are known, the capacitance of the cell membrane can be calculated. An expanded explanation of the C-M factor and DEP theory can be seen in our previous work [28].

3 Materials and methods

3.1 Cell preparation

Whole blood samples, obtained from healthy willing donors via diabetic finger stick, PC1 macrophages, MDA-MB231 breast cancer, and THP-1 leukemia cells were independently suspended in a low conductivity isotonic solution (8.5% sucrose wt/vol, 0.3% glucose wt/vol, and 0.725% RPMI wt/vol) [29]. The cells were spun down a minimum of two times at 3100 rpm for 5 min to remove any residual hematocrit or culture media such that the conductivity of the samples was $115 \pm 15\ \mu\mathrm{S\,cm^{-1}}$ as measured with a SevenGo Pro conductivity meter (Mettler-Toledo, Columbus, OH, USA). The radii for each cell type were measured using a Vi-CELL XR (Beckman Coulter, Miami, FL, USA).

3.2 Device fabrication

A silicon master stamp was fabricated on a <100> silicon substrate using photolithography. Deep Reactive Ion Etching (DRIE) was used to etch the silicon master stamp to a depth of

50 μm. Surface roughness was reduced by etching the wafer in tetramethylammonium hydroxide (TMAH) for 5 min. Finally, a thin layer of Teflon was deposited to facilitate stamp removal using typical DRIE passivation parameters. Liquid-phase polydimethylsiloxane (PDMS) in a 10:1 ratio of monomers to curing agent was degassed under vacuum prior to being poured onto the silicon master and cured for 15 min at 150°C. Fluidic connections to the channels were punched into the PDMS using 1.5 mm core borers (Harris Uni-Core, Ted Pella., Redding, CA, USA). Glass microscope slides (75 mm × 75mm × 1.2 mm, Alexis Scientific, Tracy. California, USA) were cleaned with soap and water, rinsed with distilled water, ethanol, isopropyl alcohol, and then dried with compressed air. The PDMS replica was bonded to clean glass after treating with air plasma for 2 min in a PDC-001 plasma cleaner (Harrick Plasma, Ithaca, NY, USA).

3.3 Device geometry

The device, shown in Fig. 1A, consists of a bifurcated sample channel, and three fluid electrode channels. The sample channel contains six saw-tooth features which reduce the total width of the channel from 500 to 100 μm. These features produce asymmetric electric field non-uniformities which act to push the cells toward the top or bottom of the channel. The source and sink electrodes are separated by 1.2 cm. There are two source electrode channels which are each approximately 3 cm long with a minimum width of 300 μm. The barriers separating the source electrodes from the sample channel are 20 μm thick for approximately 5.8 mm on top and bottom. The sink electrode channel is approximately 3.7 cm long with a minimum width of 300 μm. The barrier separating the sink electrode channel from the sample channel is 20 μm thick for approximately 1.6 cm.

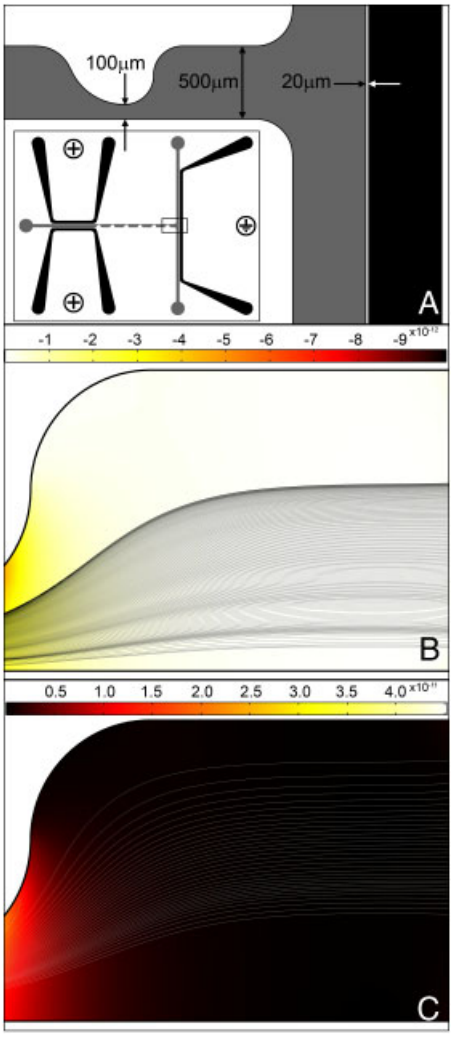

Figure 1. (A) Schematic of the low-frequency contactless DEP device. The fluid electrodes and sample channel are shown in black and grey, respectively. Particle-independent DEP vector (EV^2m^{-3}) and particle trajectories for 200 MDA-MB231 cells at (B) 10 kHz and (C) 70 kHz. 84% of particles intersected the top of the channel in (C) indicating that a large number of cells will travel along the upper wall.

3.4 Simulations

Numerical simulations were conducted to determine the relative effects of DEP and drag forces acting on the cancer cells. The electric field distribution was modeled numerically in COMSOL Multiphysics 4.1 using the AC/DC module (COMSOL, Burlington, MA, USA) by solving for the potential distribution. The boundary conditions were prescribed uniform potentials of 100 V at the inlets of the source electrode channels and as ground at the inlets of the sink electrode channels. The fluid dynamics were modeled using the laminar flow module. The inlet boundary condition was prescribed as a constant velocity of 50 μm/s as calculated based on the experimental flow rate and the cross-sectional area of the device. The outlet boundary conditions were prescribed as no pressure boundaries.

The values for the electrical conductivity and permittivity of the PDMS, sample media, and PBS that were used in this numerical modeling were similar to those reported earlier [30, 31]. The sample media and PBS had a permittivity of $80\varepsilon_0$ as assumed based on water content. The conductivity of the sample media and PBS were defined as 1.4 and 0.01 (S/m), respectively. The permittivity and conductivity of the PDMS were defined as $2.7\varepsilon_0$ and 8.33×10^{-13} (S/m), respectively. Inside the sample channel Γ was investigated for frequencies between 100 Hz and 1 GHz. The C-M factor for each cell type was calculated in MATLAB (Version R2010a, MathWorks, Natick, MA, USA) using the single shell model and the parameters found in Table 1.

3.5 Experimental parameters

The devices were placed into a vacuum jar for at least 30 min prior to experiments. The side channels were filled with

Table 1. Literature, measured, and calculated values of dielectric properties used to calculate the C-M factor and membrane capacitance for MDA-MB231, THP-1, PC1, and RBCs

MDA-MB231		THP-1	PC1	RBC	
Literature values					
ε_M	$80\varepsilon_0$[a)]	$80\varepsilon_0$[a)]	$80\varepsilon_0$[a)]	$80\varepsilon_0$[a)]	
ε_c	$50\varepsilon_0$[b)]	$162.0\varepsilon_0$[c)]	$91.6\ \varepsilon_0$[c)]	$212\ \varepsilon_0$[d)]	
σ_M	0.01[e)]	0.01[e)]	0.01[e)]	0.01[e)]	S/m
σ_c	1.00[b)]	0.66[c)]	0.46[c)]	0.40[d)]	S/m
C_m	0.0163[f)]	0.0196[c)]	0.0110[c)]	0.00997[g)]	F/m^2
R	8.88 ± 0.818[e)]	7.30 ± 0.966[e)]	6.99 ± 1.17[e)]	3.2[g)]	μm
Measured and calculated values					
σ_M	0.0117	0.0104	0.0122	0.0180	S/m
f_{xo1}	19 545	18 651	30 797	69 774	Hz
C_m	0.01518 ± 0.0013	0.01719 ± 0.0020	0.01275 ± 0.0018	0.01089[h)]	F/m^2

a) An assumption based on water content.
b) Values derived from [37].
c) Values derived from [36].
d) Values derived from [35].
e) An assumption based on measurements.
f) Values derived from [34].
g) Values derived from [38].
h) Approximated as a spherical particle with radius of 3.20 μm.

PBS, and then aluminum electrodes were placed in each side channel inlet. Teflon tubing (22 gauge) was inserted into the inlet and outlets of the main channel. The inlet tubing was connected to a 1 mL syringe containing the cell suspension via a blunt needle.

Cell suspensions were driven through the sample channel at a rate of 0.005 mL/h by a syringe pump (PHD Ultra, Harvard Apparatus, Holliston, MA, USA). An inverted light microscope (Leica DMI 6000B, Leica Microsystems, Bannockburn, IL, USA) was used to monitor the cells. For all cell types, 200 V_{RMS} was applied at frequencies between 10 and 70 kHz in increments of 10 kHz using a Trek Model 2205 high-voltage amplifier (Trek, Medina, New York, USA). For RBCs, which did not exhibit a strong DEP response at 200 V_{RMS}, an additional set of experiments were recorded at 300 V_{RMS}.

For each data point the voltage was applied for five minutes to allow for any transient responses to pass, and then a two-minute video was recorded. MATLAB was used to analyze the video from each experiment. Each frame was converted into a grey-scale image and the location of each cell was recorded as it passed through a line from top to bottom of the channel. Data from each video was normalized to determine the distribution of cells within the channel. The location, from bottom to top, at which the cells were divided into equal populations was then determined as a function of frequency. The value of f_{xo1} for each cell type was determined by finding the frequency at which the centerline of the channel split the cells into equal populations.

4 Results and discussion

4.1 Numerical results

The single shell model of the C-M factor is a complex function involving the electrical properties of the suspending media, cell membrane, and cytoplasm. Membrane capacitance, cytoplasmic conductivity, relative cytoplasmic permittivity, medium conductivity, relative medium permittivity, and cell radius impact the frequency response of the C-M factor. A sensitivity analysis of some of these parameters is shown in Supporting Information Fig. 1, and a full analysis can be seen in previous work by Docoslis et al. [32]. As presented in Eq. (3), variations in media conductivity, cell radius, and membrane capacitance alter the location of f_{xo1}. Experimentally, f_{xo1}, media conductivity, and cell radius can be measured providing the necessary parameters to calculate membrane capacitance.

As shown in Fig. 2A, the C-M factor for MDA-MB231 and THP-1 cells are nearly identical between 100 Hz and 10 MHz while the PC1 and RBCs have distinct C-M factor curves. The total force acting on each cell type is shown in Fig. 2B. These values were calculated using Eq. (1) with the values from the C-M factors in Fig. 2A, Table 1, and the values for Γ as described below. Although the C-M factor for MDA-MB231 and THP-1 cells are similar, the force acting

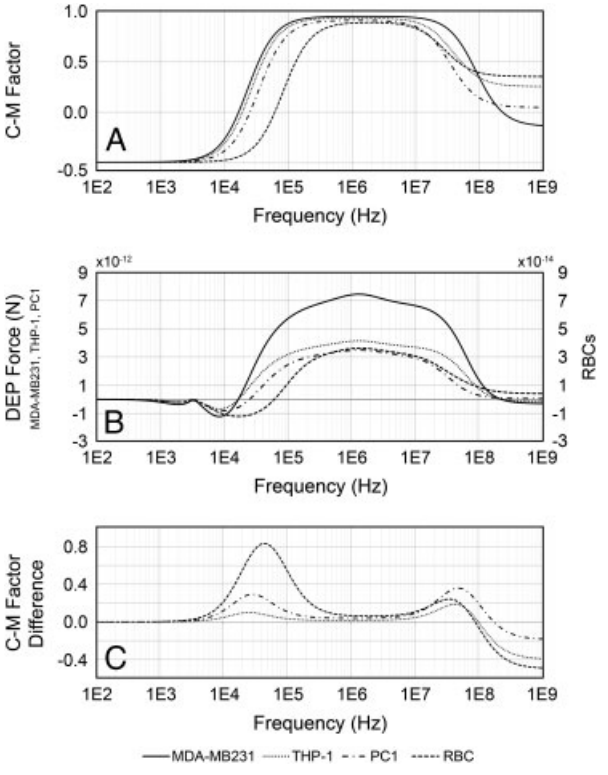

Figure 2. (A) Clausius–Mossotti factor (B) frequency-dependent force and (C) difference in the C-M factor between MDA-MB231 (solid) and THP-1 (dotted), PC1 (dash-dot), and RBCs (broken line).

on these cells is different, due to variances in their membrane capacitance and radius. The PC1 and RBCs are smaller than the cancerous cells and the total force acting on them is significantly lower. Numerically, the RBCs will experience a DEP force two orders of magnitude lower than the PC1 cells. This was manifested experimentally as the RBCs did not exhibit a significant DEP response until 300 V_{RMS} was applied.

Figure 2C shows the difference in C-M factor between the MDA-MB231 cell line and THP-1, PC1, and RBCs. There are two regions in the frequency spectrum where the C-M factor for these cells differs significantly. The first region occurs between 10 and 100 kHz and the second above 10 MHz. Typically, cDEP devices have a narrow operating region between 100 kHz and 1 MHz [31]. Below this range, the impedance of the insulating barriers dominates the system and cell manipulation is not possible. Above this range, the electronics necessary to produce voltages in excess of 100 V_{RMS} become impractical.

The cDEP device geometry in Fig. 1A was designed to operate at frequencies below 100 kHz while using a physiologically relevant sample media. As determined by our previous work in low frequency cDEP [33], a design goal of producing Γ above 1×10^{12} (V^2/m^3) was used to represent a significant value for cell manipulation. Briefly, this goal was achieved by increasing the total length of the insulating barriers and by increasing the distance between the source and sink fluid electrodes. Increasing the barrier length creates a larger capacitance which acts to decrease the total impedance of the barriers at lower frequencies. Increasing the distance between the fluid electrodes raises the resistance of the sample channel resulting in a larger proportion of the voltage drop to occur across the sample.

For this device, a constant trend was observed, independent of sample conductivity or barrier thickness. At low frequencies, the impedance of the insulating membrane between the sample channel and the fluid electrodes is very large resulting in a substantial portion of the applied voltage to drop across the barriers. As frequency increases, the capacitive nature of the barriers causes their net impedance to drop, allowing a higher proportion of the voltage drop to occur over the length of the sample channel resulting in a relatively constant Γ value over a large frequency range.

cDEP devices are analogous to a series network of resistor–capacitor pairs and changes to the conductivity of the media and barrier thickness alter the frequency response of the devices. For sample media with low conductivities, similar to deionized water, the impedance of the sample channel is large, allowing a significant voltage drop to occur across the sample at lower frequencies. As sample conductivity is increased, shown in Fig. 3A, the frequency at which significant Γ values are produced is shifted higher. Similarly, decreasing the thickness of the insulating membranes reduces their impedance and the proportion of the voltage drop that occurs across them. As shown in Fig. 3B, this allows the barriers to be overcome at lower frequencies resulting in a rise to the maximum Γ value at a lower frequency. An optimized device will utilize the lowest conductivity, physiologically acceptable sample media and the thinnest insulating membrane practically fabricated. The experiments presented here used a physiological buffer with a conductivity of approximately 100 μS/cm and devices with barrier thickness of 20 μm resulting in significant Γ values at frequencies between 10 kHz and 100 MHz.

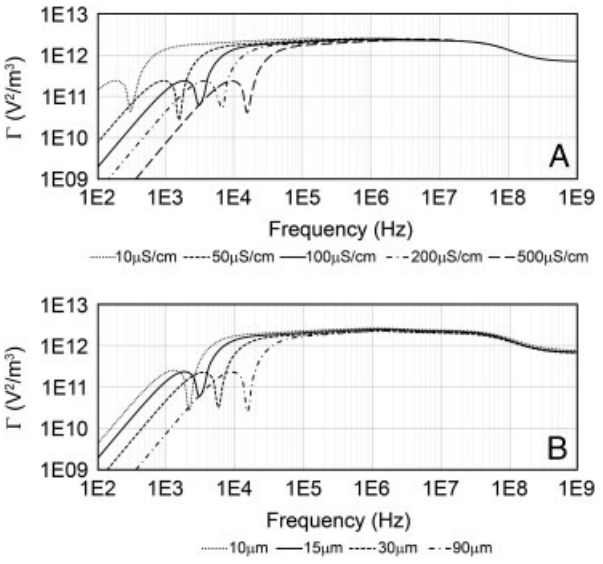

Figure 3. Parametric analysis of device performance varying (A) sample conductivity and (B) barrier thickness. Nominal values are: barrier thickness = 15 μm and sample conductivity = 100 μs/cm

Computational modeling of the device (Fig. 1B and C) indicates that the cells experience a negligible DEP force within the majority of the channel. The regions of highest DEP force occur in proximity to the constrictions. At 10 kHz, MDA-MB231 cells experience a maximum negative DEP force of approximately 1.0×10^{-12} (N). At 70 kHz, the same cells will experience a maximum positive DEP force of approximately 5.0×10^{-12} (N). The streamlines, representing MDA-MB231 cells, indicate that at low frequencies, when the C-M factor is negative, the distribution of cells is shifted toward the bottom of the channel. Although the largest non-uniformities in the electric field occur in proximity to the top wall, there is also a region of non-uniform electric field near the bottom of the channel. Numerically, this is manifested as a small depletion zone which forms near the bottom of the channel. At higher frequencies, where the C-M factor is positive, the distribution of cells is shifted toward the top of the channel. A total of 200 streamlines were simulated for an electric field of 200 V_{RMS} at 70 kHz. Eighty-four percent intersected the top wall indicating that for this frequency a large number of cells should be forced into a narrow region at the top of the channel.

4.2 Experimental results

At 10 kHz, all cell types exhibited a negative DEP response. Figure 4A shows the distribution of all cell types at 10 kHz. The net effect was to force the distribution of cells toward the bottom of the channel with most of the cells passing below the center line. A large depletion region near the bottom wall exists for MDA-MB231, THP-1, and PC1 cells. Due to their smaller size, a more narrow depletion region was observed for the RBCs. At 10 kHz, lysing of some THP-1 and PC1 cells was also observed. Negative DEP, acting on THP-1 cells (200 V_{RMS} at 10 kHz), is shown in Fig. 4C.

At frequencies above 50 kHz, all cells except RBCs exhibited a positive DEP response. Theoretically, the magnitude of the C-M factor for positive DEP can be twice that for negative DEP. Experimentally, this resulted in cells occupying a much narrower region of the device when experiencing a strong positive DEP force. As the frequency was increased above f_{xo1} for each cell type, the cells occupied a narrowing region of the top half of the channel. At 70 kHz, the MDA-MB231, THP-1, and PC1 cells occupied a region approximately 50 μm wide adjacent to the wall at the top of the channel as shown in Fig. 4B. Positive DEP, acting on THP-1 cells (200 V_{RMS} at 70 kHz), is shown in Fig. 4D.

Figure 4E shows the location which splits the cells into equal populations as a function of frequency. MDA-MB231 and THP-1 cells exhibited a similar behavior. At 10 kHz, both cell types experienced a negative DEP force which progressed the cells into the bottom half of the channel. At 20 kHz, each exhibited a slight positive DEP response indicating that their respective f_{xo1} occurred between 10 and 20 kHz. As expected by numerical calculation of their C-M factors, the transition from negative to positive DEP occurred over a narrow frequency range. Between 40 and 70 kHz the MDA-MB231 and THP-1 cells exhibited a strong positive DEP response and generally occupied a narrow region at the top of the channel. The PC1 cells exhibited a negative DEP response between 10 and 30 kHz with a sharp transition to positive DEP at 40 kHz. At 300 V_{RMS}, the RBCs

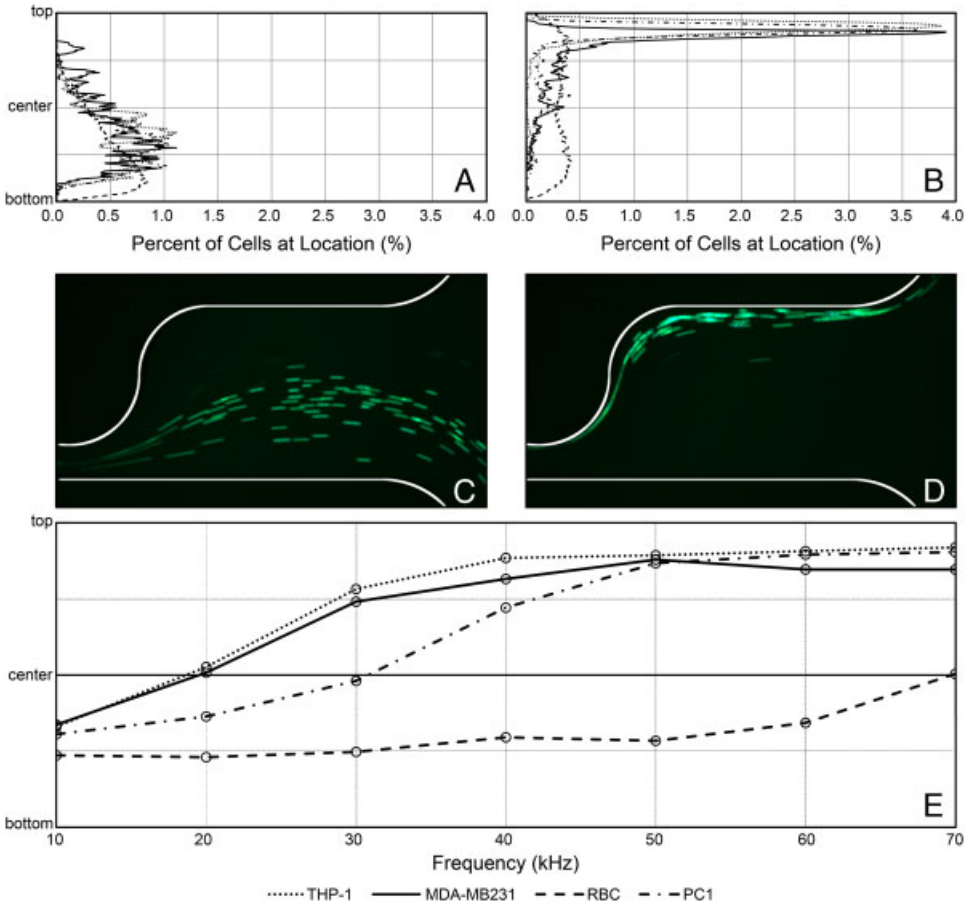

Figure 4. (A) The action of negative DEP forces the distribution of cells toward the bottom of the channel at 10 kHz. (B) At 70 kHz all cells experience positive DEP which distributes the cells toward the top of the channel. At this frequency, the distribution of RBCs is shifted only slightly above center. (C) Negative and (D) positive DEP are shown acting on THP-1 cells at 10 and 70 kHz (200 V_{RMS}), respectively. (E) Distribution of cells within the sample channel as a function of frequency. The lines indicate the location at which the cells are split into two equal populations. f_{xo1} for each cell type is the frequency at which the distribution crosses the center line.

exhibited a negative DEP response between 10 and 60 kHz. Between 10 and 30 kHz, this acted to force the cells into the bottom 75% of the channel. Between 40 and 60 kHz, the negative DEP response began to diminish; however, the distribution remained shifted toward the bottom half of the channel. At 70 kHz, the RBCs exhibited a slight positive DEP response.

The membrane capacitance for MDA-MB231 cells determined by whole-cell impedance spectroscopy was previously reported by Han et al. to be 0.0163 ± 0.0017 (F/m^2) [34]. This value provides preliminary validation of our technique which calculates a capacitance value of 0.01518 ± 0.0013 for the MDA-MB231 cell line. The capacitance values for THP-1, PC1, and RBC lines were calculated to be 0.01719, 0.01275, and 0.01089 (F/m^2). It should be noted RBCs were approximated as a spherical particle of radius 3.20 μm. The values used to for the calculations and the membrane capacitance for each cell type can be seen in Table 1.

5 Concluding remarks

This work presents the first successful use of cDEP to manipulate mammalian cells at frequencies where the C-M factor is both positive and negative. Numerical calculations of the C-M factor suggest that mammalian cells will experience similar DEP responses over a broad frequency spectrum with the exception of the regions in proximity to the first and second cross-over frequencies. The electronics necessary to produce high-voltage signals above 1 MHz are impractical, making the development of cDEP devices which operate near the first cross-over frequency necessary if this technique is to gain acceptance in laboratory and clinical settings.

The procedure presented here provides a simple way to examine the specific membrane capacitance of mammalian cells which can easily be translated into an automated process. Changes in membrane capacitance have been previously reported as an indicator of the invasiveness of certain cancers [34] and a similar cDEP device could potentially be used as an indicator of patient health by examining cells taken from biopsy or found as CTCs. The ability to analyze cells of interest and develop predictive numerical models will enable the development of future DEP devices and ultimately improve patient outcomes through the development of early cancer detection techniques.

This work was supported in part by the Institute for Critical Technology and Applied Science (ICTAS) at Virginia Tech. The authors would like to thank the members of the BEMS laboratory, especially Andrea Rojas and Harsha Kittur, for their help with editing this document.

Sano and Davalos have a pending patent in Contactless Dielectrophoresis.

6 References

[1] Borgatti, M., Rizzo, R., Mancini, I., Fabbri, E., Baricordi, O., Gambari, R., *Minerva Biotechnol.* 2007, *19*, 71–74.

[2] Del Bene, F., Germani, M., De Nicolao, G., Magni, P., Re, C. E., Ballinari, D., Rocchetti, M., *Cancer Chemother. Pharmacol.* 2009, *63*, 827–836.

[3] Ntouroupi, T. G., Ashraf, S. Q., McGregor, S. B., Turney, B. W., Seppo, A., Kim, Y., Wang, X., Kilpatrick, M. W., Tsipouras, P., Tafas, T., Bodmer, W. F., *Br. J. Cancer* 2008, *99*, 789–795.

[4] Sarantseva, S. V., Schwarzman, A. L., *Russian J. Genet.* 2009, *45*, 761–770.

[5] Tatosian, D. A., Shuler, M. L., *Biotechnol. Bioeng.* 2009, *103*, 187–198.

[6] Kawasaki, E. S., Clark, S. S., Coyne, M. Y., Smith, S. D., Champlin, R., Witte, O. N., McCormick, F. P., *Proc. Natl. Acad. Sci.USA* 1988, *85*, 5698–5702.

[7] Mostert, B., Sleijfer, S., Foekens, J. A., Gratama, J. W., *Cancer Treat. Rev.* 2009, *35*, 463–474.

[8] Hayes, D. F., Cristofanilli, M., Budd, G. T., Ellis, M. J., Stopeck, A., Miller, M. C., Matera, J., Allard, W. J., Doyle, G. V., Terstappen, L., *Clin. Cancer Res.* 2006, *12*, 4218–4224.

[9] Budd, G. T., Cristofanilli, M., Ellis, M. J., Stopeck, A., Borden, E., Miller, M. C., Matera, J., Repollet, M., Doyle, G. V., Terstappen, L. W. M. M., Hayes, D. F., *Clin. Cancer Res.* 2006, *12*, 6403–6409.

[10] Osman, I., Kang, M., Lee, A., Deng, F. M., Polsky, D., Mikhail, M., Chang, C., David, D. A., Mitra, N., Wu, X. R., Sun, T. T., Bajorin, D. F., *Int. J. Cancer* 2004, *111*, 934–939.

[11] Galan, M., Vinolas, N., Colomer, D., Soler, G., Munoz, M., Longaron, R., Ventura, P. J., Gascon, P., Estape, J., *Anticancer Res.* 2002, *22*, 2877–2884.

[12] Dingemans, A. M. C., Brakenhoff, R. H., Postmus, P. E., Giaccone, G., *Lab. Invest.* 1997, *77*, 213–220.

[13] Berteau, P., Dumas, F., Gala, J. L., Eschwege, P., Lacour, B., Philippe, M., Loric, S., *Clin. Chem.* 1998, *44*, 1750–1753.

[14] Berteau, P., Dumas, F., Gala, J. L., Eschwege, P., Lacour, B., Philippe, M., Loric, S., *Clin. Chem.* 1998, *44*, 677–679.

[15] Koike, E., Yamashita, H., Noguchi, S., Ohshima, A., Watanabe, S., Uchino, S., Arita, T., Kuroki, S., Tanaka, M., *Endoscopy* 2002, *34*, 457–460.

[16] Schroder, C. P., Ruiters, M. H. J., de Jong, S., Tiebosch, A., Wesseling, J., Veenstra, R., de Vries, J., Hoekstra, H. J., de Leij, L., de Vries, E. G. E., *Int. J. Cancer* 2003, *106*, 611–618.

[17] Traweek, S. T., Liu, J., Battifora, H., *Am. J. Pathol.* 1993, *142*, 1111–1118.

[18] Pohl, H. A., *J. Appl.Phys.* 1951, *22*, 869–871.

[19] Cummings, E. B., Singh, A. K., *Anal. Chem.* 2003, *75*, 4724–4731.

[20] Lapizco-Encinas, B. H., Davalos, R. V., Simmons, B. A., Cummings, E. B., Fintschenko, Y., *J. Microbiol. Methods* 2005, *62*, 317–326.

[21] Chen, K. P., Pacheco, J. R., Hayes, M. A., Staton, S. J. R., *Electrophoresis* 2009, *30*, 1441–1448.

[22] Masuda, S., Itagaki, T., Kosakada, M., *IEEE Trans. Industry Appl.* 1988, *24*, 740–744.

[23] Becker, F. F., Wang, X. B., Huang, Y., Pethig, R., Vykoukal, J., Gascoyne, P. R. C., *J. Phys. D – Appl. Phys.* 1994, *27*, 2659–2662.

[24] Shafiee, H., Caldwell, J. L., Sano, M. B., Davalos, R. V., *Biomed. Microdev.* 2009, *11*, 997–1006.

[25] Shafiee, H., Sano, M. B., Henslee, E. A., Caldwell, J. L., Davalos, R. V., *Lab Chip* 2010, *10*, 438–445.

[26] Pohl, H. A., Plymale, C. E., *J. Electrochem. Soc.* 1960, *107*, 390–396.

[27] Foster, K. R., Sauer, F. A., Schwan, H. P., *Biophys. J.* 1992, *63*, 180–190.

[28] Henslee, E. A., Sano, M. B., Rojas, A. D., Davalos, R. V., *Electrophoresis* 2011, *32*, 2523–2529.

[29] Flanagan, L. A., Lu, J., Wang, L., Marchenko, S. A., Jeon, N. L., Lee, A. P., Monuki, E. S., *Stem Cells* 2008, *26*, 656–665.

[30] Shafiee, H., Caldwell, J. L., Sano, M. B., Davalos, R. V., *Biomed. Microdevices* 2009, *11*, 997–1006.

[31] Shafiee, H., Sano, M. B., Henslee, E. A., Caldwell, J. L., Davalos, R. V., *Lab Chip* 2010.

[32] Docoslis, A., Kalogerakis, N., Behie, L. A., Kaler, K., *Biotechnol. Bioeng.* 1997, *54*, 239–250.

[33] Sano, M. B., Caldwell, J. L., Davalos, R. V., *Biosens. Bioelectron.* 2011, DOI: 10.1016/j.bios.2011.07.048.

[34] Han, A., Yang, L., Frazier, A. B., *Clin. Cancer Res.* 2007, *13*, 139–143.

[35] Gimsa, J., Muller, T., Schnelle, T., Fuhr, G., *Biophys. J.* 1996, *71*, 495–506.

[36] Yang, J., Huang, Y., Wang, X. J., Wang, X. B., Becker, F. F., Gascoyne, P. R. C., *Biophys. J.* 1999, *76*, 3307–3314.

[37] Sancho, M., Martinez, G., Munoz, S., Sebastian, J. L., Pethig, R., *Biomicrofluidics* 2010, *4*.

[38] Cruz, J. M., Garcia-Diego, F. J., *J. Phys. D – Appl. Phys.* 1998, *31*, 1745–1751.

